Solid State Phenomena
ISSN: 1662-9779, Vol. 389, pp 171-180
doi:10.4028/p-OHzO30

Submitted: 2026-01-16
Revised: 2026-02-16
Accepted: 2026-02-24
Online: 2026-04-16

Hybrid Hot Forming of High-Strength Aluminum Alloys: Influence of Local Deformation on Post-Aging Mechanical Properties

Max Gröbel[1,a*], Karl J. Tilly[1,b], Emad Scharifi[1,c] and Junhe Lian[1,d]

[1]Institute of Metal Forming (IBF), RWTH Aachen University, Intzestraße 10, 52072 Aachen, Germany

[a]max.groebel@ibf.rwth-aachen.de, [b]karl.tilly@ibf.rwth-aachen.de,
[c]emad.scharifi@ibf.rwth-aachen.de, [d]junhe.lian@ibf.rwth-aachen.de

Keywords: Sheet Metal forming, Gas-based hot forming, Precipitation hardening aluminum,

Abstract. Hybrid hot sheet forming routes that integrate heat treatment within the forming tool offer a promising pathway to manufacture complex geometries from precipitation-hardenable 7xxx aluminum alloys, but the resulting local deformation and thermal histories may generate pronounced spatial property variations. In this work, a gas-based hybrid forming process is demonstrated for EN AW-7020 sheets, combining in-tool solution heat treatment, isothermal forming at 500 °C with gas calibration and active pushing, followed by water quenching and artificial aging. A thermo-mechanically coupled finite-element model is used to identify regions of distinct equivalent plastic strain in a representative demonstrator geometry and to guide local specimen extraction. Tensile tests from low- and high-strain regions reveal clear location-dependent stress-strain responses after aging, with a reduction in ultimate tensile strength exceeding 20 % in the more heavily deformed zones compared with reference material. Microstructural observations by optical microscopy indicate differences in grain morphology between component regions, consistent with the non-uniform thermo-mechanical history. The results highlight the need to account for local strain and process history when designing hybrid-formed 7xxx components and motivate targeted strategies for controlling property gradients through process parameter tuning and tailored post-forming heat treatment.

Introduction

The increasing demand for lightweight structural components in both automotive and aerospace industries has intensified research into forming processes for high-strength aluminum alloys of the 6xxx and especially the 7xxx series [1, 2]. These alloys offer excellent strength-to-weight ratios and corrosion resistance, making them promising candidates for load-bearing structures in modern mobility applications. Despite their advantageous strength-to-weight ratio, 7xxx-series alloys exhibit limited ductility at room temperature, which results in localized thinning, reduced formability, and an increased risk of crack initiation during conventional cold forming [3, 4].

Recent studies highlight that warm and hot forming routes represent a viable solution to overcome these challenges. Comprehensive reviews of hot sheet metal forming for 7xxx alloys show that hot forming at 500 °C significantly improves formability while enabling the manufacture of geometrically complex components [2]. However, warm-forming routes cause heterogeneous microstructures that require subsequent heat treatments to obtain a homogenous microstructure and the desired mechanical performance [4]. Warm sheet forming studies using precipitation hardenable aluminum alloys AA7075 and AA7020 demonstrate that temperatures between 150 °C and 300 °C increase the drawability and limit strain localization, allowing components to reach up to 90 % of the T6 strength after subsequent aging [1, 5]. Beyond conventional warm forming, hybrid thermo-mechanical process routes have gained substantial attention [6, 7]. For example, in [7], a hybrid hot forming process is developed consisting of solution heat treatment, immediate forming, quenching, and artificial aging to counteract the disadvantages of warm forming and positively influence the final properties with the integrated aging step. These developments align with industrial hot forming technologies such as Hot Forming and Quenching (HFQ®), which combines quenching and forming after solution heat treatment. In the case of precipitation hardenable aluminum alloys, artificial aging

is subsequently carried out to adjust the desired mechanical properties. HFQ®-based studies report significant springback reductions and improved dimensional accuracy for 7xxx-series alloys [8, 9]. Investigations on the forming-induced pre-deformation show that it strongly influences precipitation behavior during subsequent aging. Local pre-strain accelerates heterogeneous nucleation, lowering the achievable peak strength and altering the distribution of Guinier-Preston zones, particularly in Al-Zn-Mg alloys [5, 10]. This explains why even moderate plastic deformation can significantly reduce final strength after artificial aging [11].

However, the impact of the integrated gas-supported hot sheet forming process on the final mechanical properties of the complex-shaped components has not yet been evaluated. The present study, therefore, investigates this by means of tensile tests and grain size distribution to counteract the lack of knowledge for the combination of modern hot forming processes with the integrated heat treatment. This investigation aims to address microstructural changes to the forming operation and the mechanical properties.

Materials and Methods

The material used in this study is the high-strength aluminum alloy EN-AW 7020 in the as-received H18 condition with a hardness level of 88 HV2 and an ultimate tensile strength (UTS) of 257 MPa. Table 1 shows the chemical composition according to the supplier of the material. The sheet thickness investigated is 2 mm.

Table 1. Chemical composition of the investigated EN AW 7020

Si	Fe	Cu	Mn	Mg	Cr	Zn	Zr	Al
0.03	0.14	0.00	0.21	1.21	0.13	4.37	0.1138	remaining

Experimental setup. The setup of the process is based on the process shown in [7] consisting of a die, a punch with gas channels, and a blank holder equipped with an active pushing system to increase the draw-in, as shown in Fig. 1. The active pushing system is based on eight cylinders, every 45° to push the sheet into the die. The pushers are controlled via LabView, which synchronizes the blank-holder position with the activation of the pneumatic system. The pushing system is divided into the x-pushers and the +-pushers, which can be controlled solely. After the completion of the deep drawing, a pressure valve opens and a pressure of max. 9 bar is applied to the cylinders, resulting in a max. pusher force of 1500 N. The end plates of the pushers are manufactured from TiAl6V4 because of its high strength combined with low thermal conductivity even at high temperatures. The tooling setup enables three different procedures to be performed: deep drawing, deep drawing with gas calibration, and deep drawing with active sheet pushing, as well as gas calibration. The present study deals with the complete forming process consisting of deep drawing, pushing, and gas calibration. Moreover, this set-up enables solution heat treatment within the forming tool up to 600 °C using heating cartridges (Mickenhagen high-performance heating cartridge 500 W – 800 W) in the punch, blank holder, and die, as well as additional heating coils (Mickenhagen flexible tubular heating element 2500 W – 3320 W) in the blank holder and die. Cooling channels are integrated into the frame to thermally decouple the heated tool components and ensure process stability.

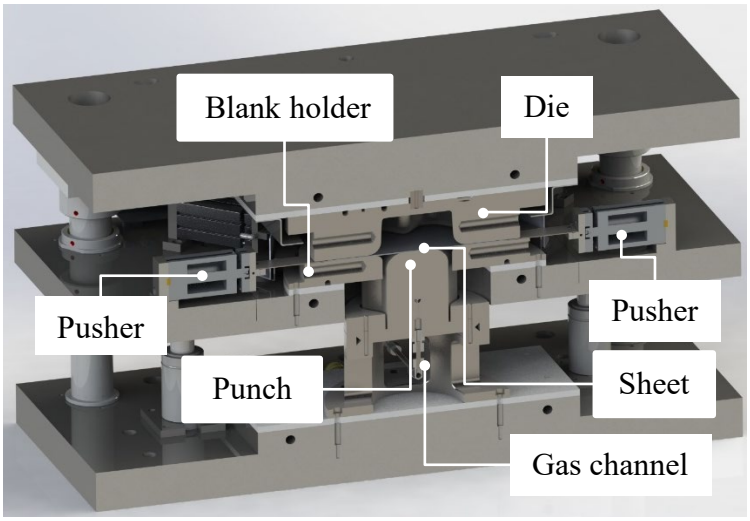

Fig. 1. Setup of the tool used for the experimental investigations

For the experimental procedure, the parts were lubricated with a graphite-based lubricant after being water cut to the proposed octagonal shape and cleaned up. To reduce the friction during hot forming, dies were lubricated as well as the pushers and the sheet material with graphite-based lubricant. The forming process is integrated into the heat treatment of the material; the sheet is placed in the center of the heated blank holder and conductively heated to the SHT temperature of 500 °C. The heat treatment is performed for 20 min to fully dissolve the alloying elements. Subsequently, the forming process starts and can be divided into two major steps. First deep drawing takes place within two seconds with a punch velocity of 30 mm/s and an increasing blank holder force of 3 kN to 6 kN applied by the gas springs, followed by the gas calibration supported by the pushing of the sheet with a force of 1500 N as shown in Fig. 2. The gas used for calibration is nitrogen with a pressure of 10 MPa.

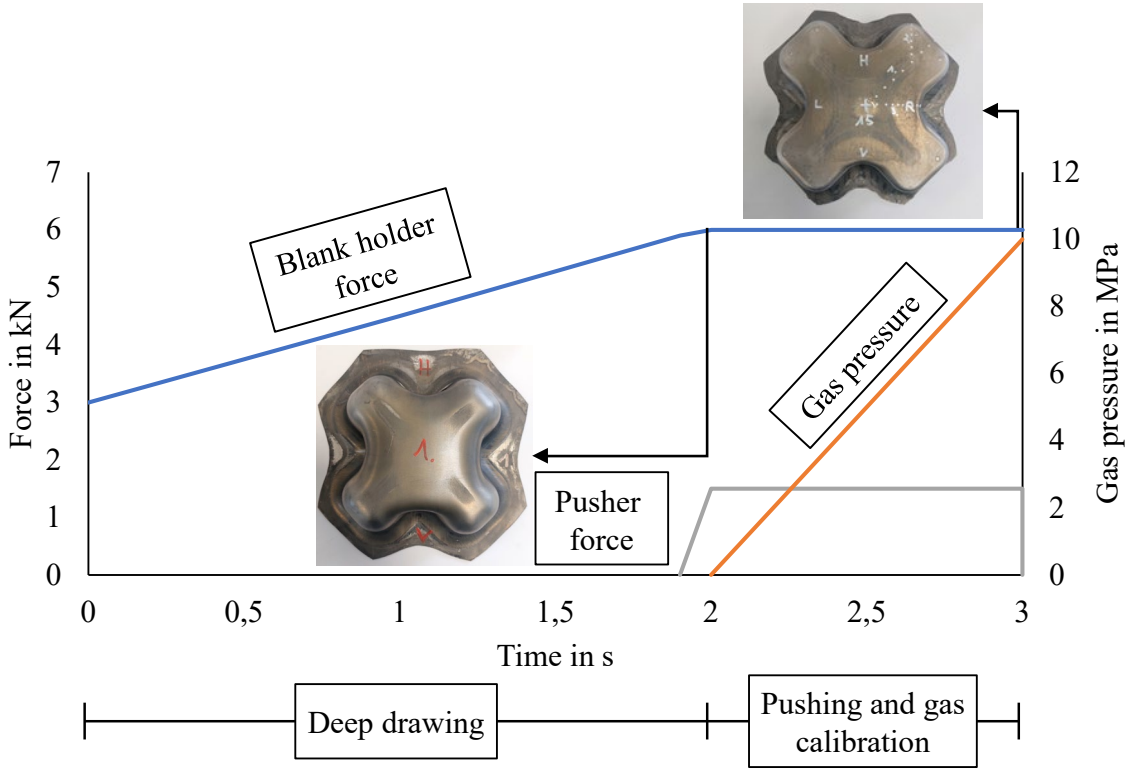

Fig. 2. Overview of the forming process and resulting parts

After fully forming, the part is directly quenched in water. To finally set the mechanical properties, the parts are artificially aged with another two-step heat treatment at 90 °C for 8 h and 145 °C for 8 h.

Fig. 3 shows the thermal reference cycle of the used alloy. For comparison, a section of sheet metal with the same temperature/time history is prepared and analyzed in the same way.

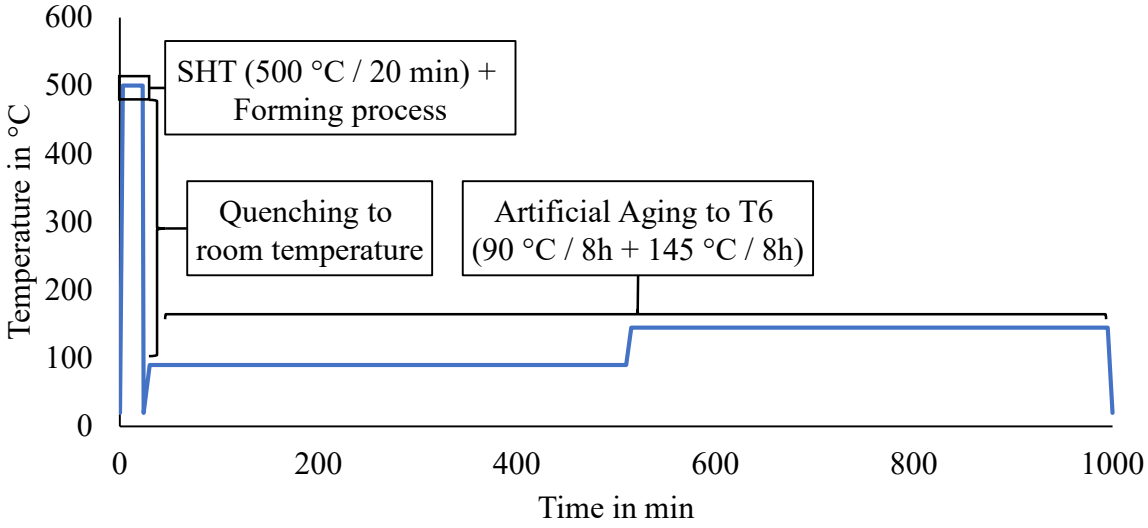

Fig. 3. Thermal reference cycle

The determination of the mechanical properties after forming is done by tensile tests. Therefore, tensile specimens are taken from identified regions by wire erosion and tested using the tensile testing machine Z100 with an optical strain measurement system by the ARAMIS-4M-system. Tests are performed at room temperature under quasistatic conditions with a crosshead speed of 0.9 mm/min for the large samples and 0.375 mm/min for the small samples, equivalent to a strain rate of 0.001 s^{-1}. Fig. 4 shows the extracted specimens; the corresponding numerical investigations for identifying the relevant regions can be found in the **results and discussion** section. Furthermore, grain size is determined by the linear intercept method. For preparation, the samples are cold-embedded, ground, polished, and finally etched using Barker's reagent.

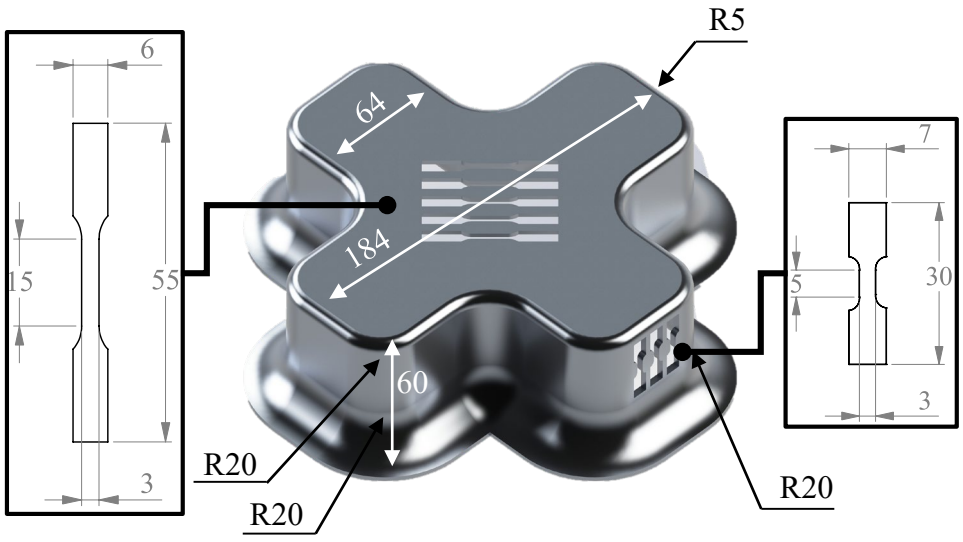

Fig. 4. Tensile specimens extracted from the completely formed cross-die (dimensions in mm)

Numerical setup. In addition to the experimental investigations, a numerical model is built in LS-DYNA R13 and pre- and post-processed in LS-PrePost 4.9 in accordance with [7]. The basic setup is shown in Fig. 5 at the beginning, during deep drawing with the pushers moving towards the sheet, and at the end of the process. Only one quarter of the setup is modelled to reduce calculation time.

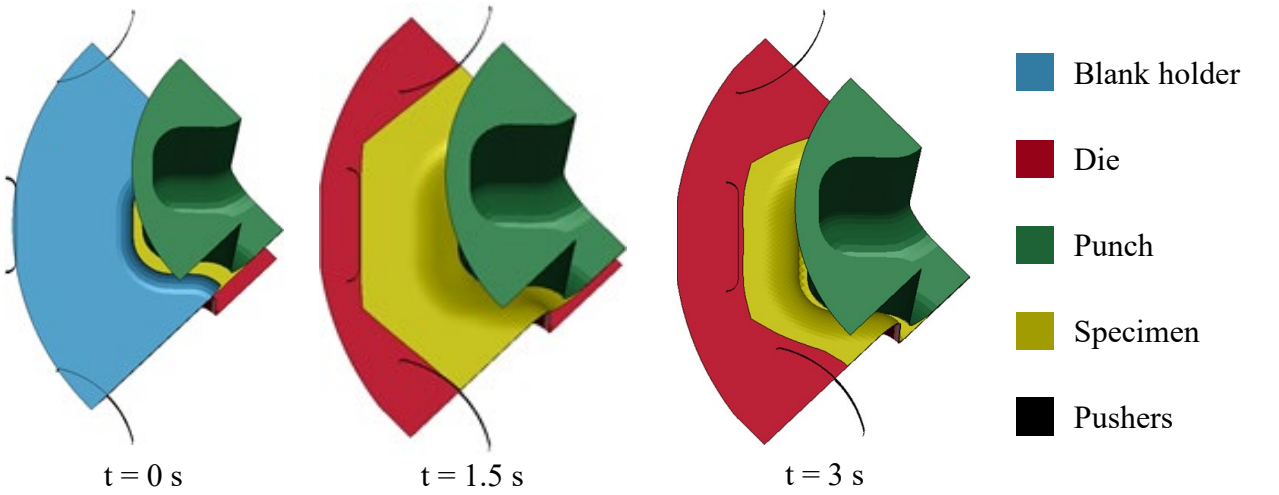

Fig. 5. Numerical model of the forming process as a function of process stage

The sheet is modeled using 3D thermal shell elements with a fully integrated formulation and nine integration points through the thickness. Die, blank holder, punch, and the pushers are also modelled using thermal shell elements with reduced integration. Mechanical properties are assigned via the Thermo_Elastic_Viscoplastic_Creep card for the sheet and with the Thermal_Isotropic_material card for all other parts. The sheet is modeled as an elasto-plastic deformable body, while all tools and pushers are treated as rigid components. The flow curves for EN AW 7020 are taken by the isothermal stacked layer compression test directly after the solution heat treatment.

The process takes three seconds to complete and is divided into the deep drawing and the assisted calibration step. The die is fixed, and the punch is moving with a velocity of 30 mm/s, resulting in a deep drawing time of two seconds to reach the full drawing. The subsequent calibration takes one second with an increasing gas pressure, and the pushers are active during the deep drawing to get in contact at the start of the calibration.

Results and Discussion

Based on the methodology described, components are successfully produced without cracks and initially numerically investigated to identify the strain distribution. Furthermore, tensile tests and grain size determination are carried out.

Local deformation behavior. With the help of the already validated numerical model from [7], local strains were extracted to identify regions with different forming histories. Fig. 6 illustrates the strain distribution of the formed part at the initial state, after deep drawing, and after subsequent gas calibration. After deep drawing, a maximum strain of $\varepsilon = 0.4$ is observed in the wall region and in the corner, whereas the bottom region remains almost undeformed.

The subsequent gas calibration step leads to a pronounced localization of deformation in the corner area, where the strain increases to a maximum value of $\varepsilon = 1.08$. This strong local strain accumulation is directly associated with a significant thickness reduction, resulting in a maximum thinning of 65 % in the corner region. In contrast, the wall region experiences a moderate but continuous increase over both forming stages, while the bottom part is only marginally affected by the overall forming process.

An analysis of the forming history reveals that the deformation mechanisms differ distinctly between the individual regions of the component. The wall deformation is mainly induced during the tool-based deep drawing step, whereas the gas calibration predominantly contributes to the additional strain and thinning in the corner region. Overall, the induced deformation after the complete forming process is significantly higher in the wall and corner regions ($\varepsilon_{\mathrm{Wall}} \geq 0.4$) compared to the bottom region ($\varepsilon_{\mathrm{Bottom}} \leq 0.05$), clearly demonstrating the strong localization effects inherent to the multi-stage forming process.

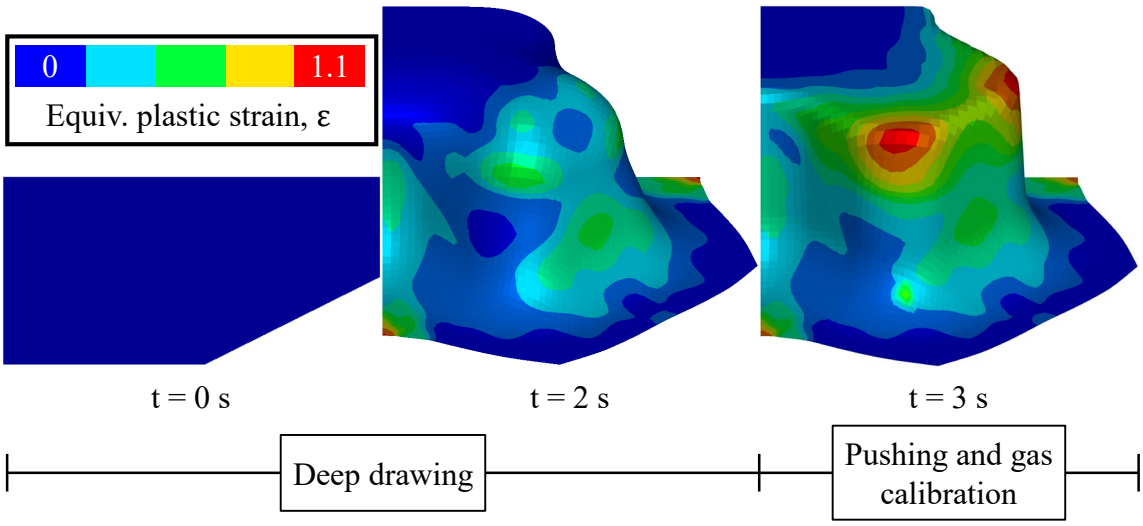

Fig. 6. Evolution of the numerically predicted strain distribution during multi-stage forming

A geometric comparison of the experimentally manufactured component with the simulation model is based on the thinning along three symmetry lines to validate the plastic flow behavior, as shown in Fig. 7. The thinning behavior and its tendencies are represented quite well by the simulation model with minor deviations in the flanging area. As shown in the numerical analysis at the end of the complete forming process, the thinning along lines 1 and 2 in the bottom radius reaches its maximum, whereas this maximum is not pronounced along line 3. The greatest thinning can be detected in the corner area, which corresponds to the results of the numerical analysis. It can be seen that gas calibration causes the greatest change in shape in the area of the arms and the corners, and significantly increases thinning in this area. Furthermore, friction between the sheet metal and the forming tool restricts material flow, causing material to flow from regions that are not previously in contact with the die. This redistribution of material subsequently results in increased local thinning.

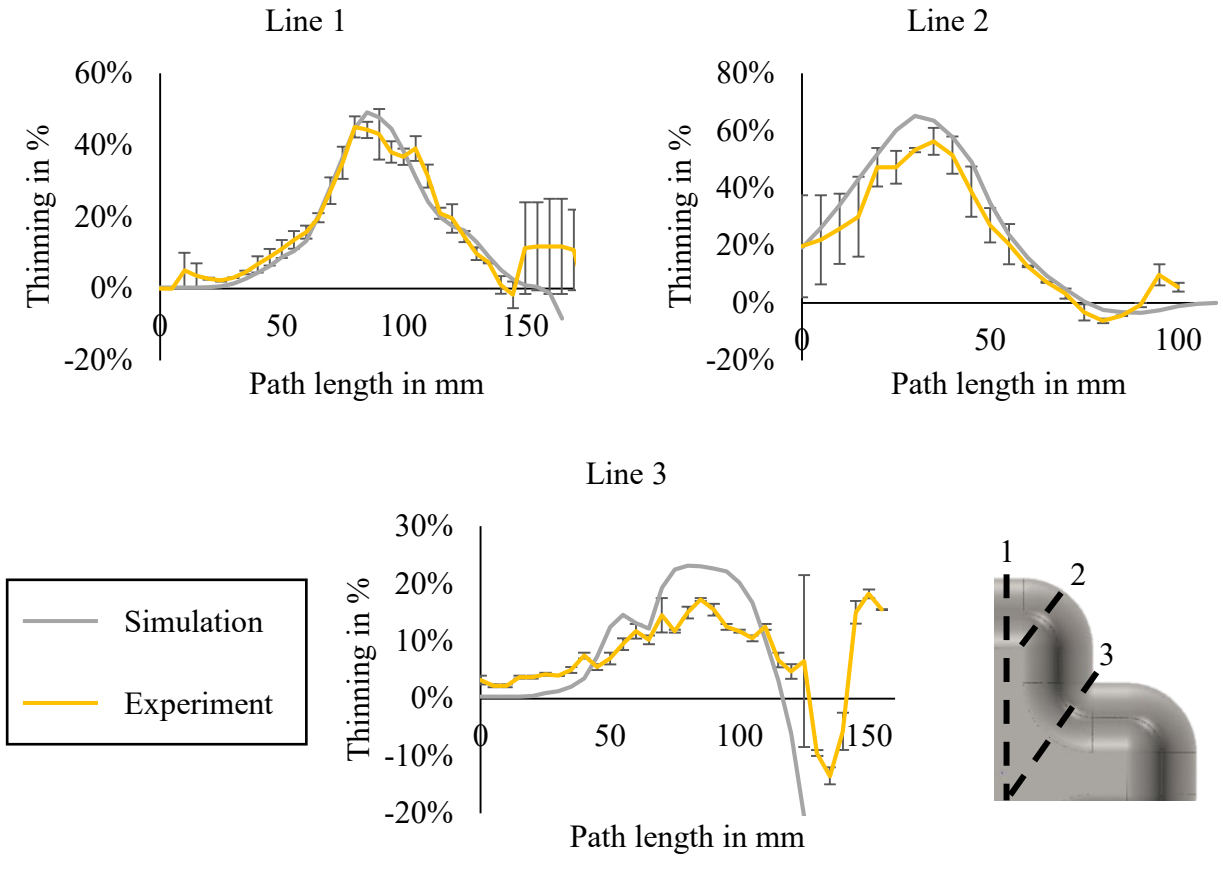

Fig. 7. Thinning comparison along three symmetry lines of the completely formed cross-die

The deviations in the flanging area are due to the fact that the model is not considering the blank holder force compressing the sheet in this zone. Also, the high punch compression force acting on the bottom is not considered within the simulation model, resulting in less thinning at the bottom (Line 1 and Line 2). For inspection of the mechanical properties, tensile tests are carried out as mentioned in the **Materials and methods** section. The specimens are taken from the bottom region and the wall region.

Tensile tests. Fig. 8 a) illustrates the tensile behavior of the Al-Zn-Mg alloy after the complete thermo-mechanical processing route, comprising solution heat treatment (SHT), gas-based forming at 500 °C, and subsequent artificial aging at 90 °C for 8 h, followed by 145 °C for an additional 8 h. The resulting engineering stress-strain curves are shown for tensile specimens extracted from different regions of the formed component, namely the wall (dotted lines) and the bottom (solid line), to capture spatial variations in the mechanical response induced by the hot forming process. For comparison, the tensile properties of the reference sample are also included in the figure to assess the influence of the forming operation on the final mechanical properties. A yield strength of at least 215 MPa is observed in all samples, while the yield strength of the cross-die specimens remains below that of the reference sample.

The tensile strength decreases with increasing deformation, with a more pronounced reduction in the wall region compared to the bottom region. The elongation at fracture decreases in the base region and deteriorates significantly in the wall region. Fig. 8 b) shows the strain hardening rate as a function of the engineering strain. Strain hardening rate is calculated using formula (1), which measures the local gradient based on the differential stress and strain.

$$\theta|_i = \left.\frac{d\sigma}{d\varepsilon}\right|_i = \frac{\sigma|_{i+1} - \sigma|_{i-1}}{\varepsilon|_{i+1} - \varepsilon|_{i-1}} \tag{1}$$

All samples exhibit a high initial strain-hardening rate followed by a continuous decrease with increasing strain. Specimens from the wall region show a more rapid decline and reach zero strain-hardening at lower strains, indicating an earlier onset of plastic instability. The black curve, representing the reference sheet material, exhibits the lowest strain-hardening rate.

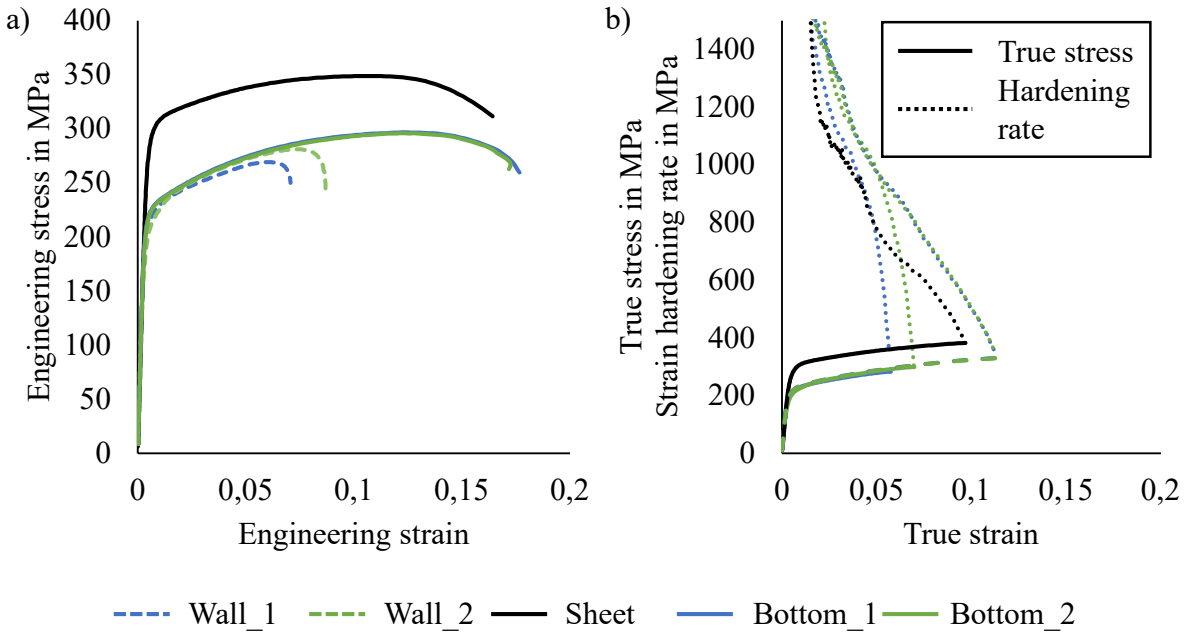

Fig. 8. True stress–strain behavior and corresponding strain hardening rate as a function of prior deformation state after artificial aging

The mechanical behavior observed in the tensile tests reflects the strong coupling between the local deformation state and the subsequent precipitation kinetics of the 7xxx alloy within the hybrid hot forming route. The reduction of the UTS in the wall area is consistent with the high local strains identified in the numerical model and shown in Fig. 6. In Al-Zn-Mg alloys, such pre-deformation is known to accelerate heterogeneous nucleation during artificial aging, thereby reducing the achievable peak strength. This mechanism explains why the wall region, despite undergoing the same artificial aging treatment as the bottom region and the reference sheet, reaches noticeably lower tensile strength values. Furthermore, the earlier decline of strain hardening in the wall specimens indicates that the material enters the softening regime sooner due to the increased density of deformation-induced defects, as shown in Fig. 8 a). These defects act as preferential nucleation sites during aging and promote the formation of coarser precipitates, thereby lowering hardenability. In contrast, the bottom area in Fig. 6 shows only minor deformation and therefore preserves a precipitation sequence closer to that of the reference sheet, resulting in higher UTS. Regions with pronounced stretching exhibit locally increased dislocation density, which further influence the precipitation behavior. The black curve, representing the reference sheet material, shows the lowest strain-hardening rate over the entire strain range. This behavior reflects the absence of forming-induced dislocation structures, resulting in a reduced work-hardening capability compared to the formed specimens. As a result, the hybrid process introduces characteristic spatial variations in mechanical properties that follow directly from the strain distribution during forming. These results indicate that local deformation during forming directly affects precipitation and work-hardening, which must be accounted for in process optimization and component design to ensure consistent mechanical performance.

Grain size determination. In addition to the tensile tests, grain size is determined. For comparison Fig. 9 shows the development of the grain structure during the thermal stages of manufacturing the part including the heat treatment for the undeformed sheet. The rolling structure can clearly be identified in the delivery condition by the horizontally stretched grains. After solution heat treatment, a homogeneous grain size distribution emerges, which remains visible even after aging. The grain size decreases by approximately 10%. This confirms that the heat treatment effectively homogenizes the microstructure, providing a consistent starting point for the forming operation.

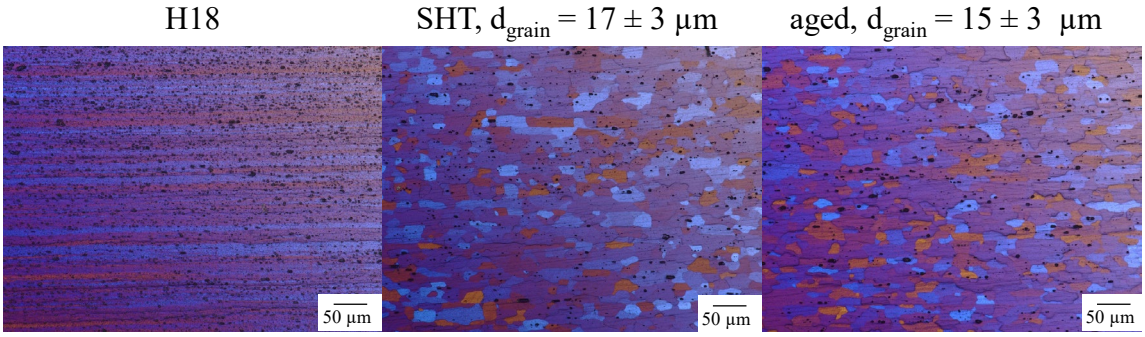

Fig. 9. Effect of heat treatment without plastic deformation on the grain size distribution of the used sheet material

o determine the influence of forming on the grain size distribution, samples are cut from the cross-die as shown in Fig. 10. The regions with maximum thinning exhibit slightly finer grains compared to the undeformed sheet, whereas areas with minimal pre-deformation as the bottom region tend to show slightly larger grains. These differences are small and close to the measurement scatter but consistent with the local deformation history. The wall region does not show measurable grain coarsening; instead, the grains appear elongated and locally refined due to the deformation introduced during forming. The corner of the cross-die is formed at the end of the process and therefore experiences the highest cooling rate due to forced convection. This rapid cooling suppresses grain growth after quenching, leading to a locally finer grain appearance relative to surrounding regions. Although no significant overall change in grain size is observed across the part, grain elongation is clearly visible in the areas of high thinning.

Fig. 9 illustrates that the microstructural variations follow the deformation history obtained from the numerical analysis in Fig. 6. The grain refinement in the highly thinned regions can be attributed to intense stretching during forming, which elongates and partially fragments the grains. This effect is most pronounced in the corner regions, where the highest cooling rates further restrict grain growth. In contrast, areas with minimal deformation as the bottom region cool more slowly, which allows for slightly more grain growth during the thermal cycle.
Overall, the combination of deformation and locally varying cooling conditions leads to a largely homogeneous grain-size distribution across the component, with regionally discernible grain elongation characteristic of hybrid hot sheet-forming processes. This uniform microstructure shows process robustness, ensuring predictable mechanical performance and consistent quality in hybrid hot sheet-forming of single components.

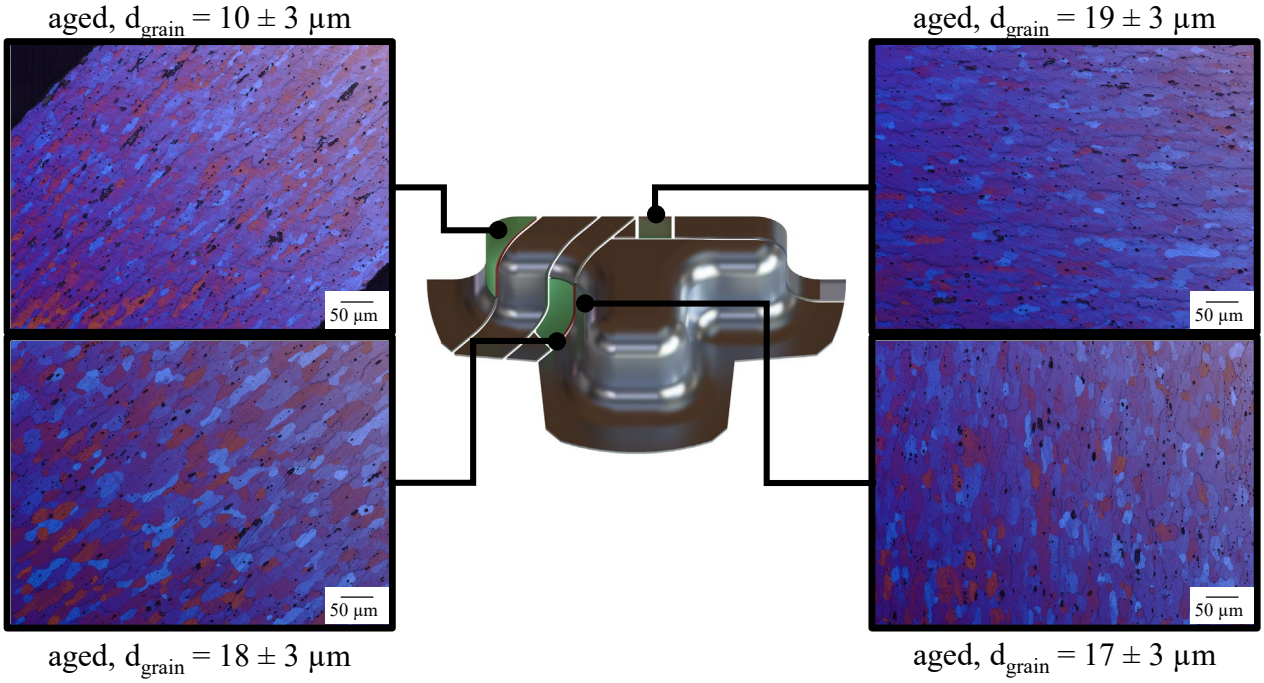

Fig. 10. Regional influence on post-ageing grain size distribution within the cross-die

Summary

Within this study the influence of forming on mechanical properties of the precipitation hardenable aluminum alloy EN AW 7020 has been investigated on the hybrid hot sheet forming process [7]. To determine relevant regions and correspond them to the mechanical properties, a numerical identification was carried out. Based on the obtained results the following key findings can be drawn:

- The forming operation followed by the artificial aging reduces the ultimate tensile strength. It can be stated that the degree of plastic deformation further reduces the UTS, lowering the UTS more than 20 % compared to the non-deformed sheet.
- Grain refinement can only be observed in regions with maximum thinning, resulting in elongation of grains. This elongation can also be observed in the wall regions due to the stretching.
- The hybrid hot sheet forming process introduces characteristic mechanical and microstructural gradients that directly correlate with the local strain distribution. These gradients must be considered in the design of load-bearing components made from 7xxx aluminum alloys.

Further research should focus on the detailed influence of pre-deformation on precipitation kinetics and local hardness evolution in EN AW 7020. Optimizing hybrid hot forming parameters, such as temperature, strain rate, and cooling, could help reduce UTS loss and control grain growth. The correlation between microstructural gradients and mechanical performance, including fatigue and

fracture behavior, should be further investigated. Finally, predictive models and design guidelines for load-bearing components made from 7xxx aluminum alloys could be developed based on these findings.

Acknowledgements

This project (Lightness.NRW) was funded by "Europäischer Fonds für regionale Entwicklung" (EFRE). The authors of IBF further acknowledge excellent collaboration with the project partners SMS group GmbH, Ford-Werke GmbH, Hydro Extruded Solutions GmbH, Hydro Aluminum Rolled Products GmbH, HoDforming GmbH, CTES and Automotive Laboratory of FH Aachen. The authors would like to thank Stefan Seidel for the preparation of the tensile specimens.

References

[1] W.-L. Chen and R.-S. Lee, Novel Aging Warm-Forming Process of Al-Zn-Mg Aluminum Alloy Sheets and Influence of Precipitate Characteristics on Warm Formability. Metals, 8 (2024) 844.

[2] M. Skwarski, A review of sheet warm forming methods for high-strength 7xxx aluminum alloys. Materials Science-Poland, 3 (2025) 64–84.

[3] M. Kumar, N. Sotirov, and C. M. Chimani, Investigations on warm forming of AW-7020-T6 alloy sheet. Journal of Materials Processing Technology, 8 (2014) 1769–1776.

[4] K. Zheng, D. J. Politis, L. Wang, and J. Lin, A review on forming techniques for manufacturing lightweight complex—shaped aluminium panel components. International Journal of Lightweight Materials and Manufacture, 2 (2018) 55–80.

[5] J. A. Österreicher, M. A. Tunes, F. Grabner, A. Arnoldt, T. Kremmer, S. Pogatscher, and C. M. Schlögl, Warm-forming of pre-aged Al-Zn-Mg-Cu alloy sheet. Materials & Design (2020) 108837.

[6] S. Lotz, E. Scharifi, U. Weidig, and K. Steinhoff, Effect of Combined Forming and Aging Processes on the Mechanical Properties of the Precipitation-Hardenable High-Strength Aluminum Alloys AA6082 and AA7075. Metals, 8 (2022) 1250.

[7] N. K. Baru, T. Teeuwen, D. Bailly, and E. Scharifi, A novel hybrid hot forming process concept for high strength aluminum alloys. Materials Research Proceedings, 52 (2025) 134–141.

[8] R. Wu, W. Dai, J. Luo, M. Li, Y. Liu, and H. Li, Aluminum Alloy Hot Stamping and Forming Technology: A Review. Materials (Basel, Switzerland), 8 (2025).

[9] E. Scharifi, V. A. Yardley, U. Weidig, D. Szegda, J. Lin, and K. Steinhoff, Hot Sheet Metal Forming Strategies for High-Strength Aluminum Alloys: A Review—Fundamentals and Applications. Adv Eng Mater, 16 (2023).

[10] M. C. Paulisch, N. Wanderka, M. Haupt, S. Selve, I. Driehorst, and W. Reimers, The influence of heat treatments on the microstructure and the mechanical properties in commercial 7020 alloys. Materials Science and Engineering: A (2015) 254–262.

[11] A. Deschamps, F. Livet, and Y. Bréchet, Influence of predeformation on ageing in an Al–Zn–Mg alloy—I. Microstructure evolution and mechanical properties. Acta Materialia, 1 (1998) 281–292.

The publication of this article was funded by the RWTH Aachen University 10.13039/501100007210